Edge Properties and Majorana Fermions in the Proposed Chiral d-Wave Superconducting State of Doped Graphene

Annica M. Black-Schaffer

Department of Physics and Astronomy, Uppsala University, Box 516, S-751 20 Uppsala, Sweden

(Received 11 April 2012; published 7 November 2012)

We investigate the effect of edges on the intrinsic d-wave superconducting state in graphene doped close to the van Hove singularity. While the bulk is in a chiral $d_{x^2-y^2} + id_{xy}$ state, the order parameter at any edge is enhanced and has $d_{x^2-y^2}$-symmetry, with a decay length strongly increasing with weakening superconductivity. No graphene edge is pair breaking for the $d_{x^2-y^2}$ state, and there are no localized zero-energy edge states. We find two chiral edge modes which carry a spontaneous, but not quantized, quasiparticle current related to the zero-energy momentum. Moreover, for realistic values of the Rashba spin-orbit coupling, a Majorana fermion appears at the edge when tuning a Zeeman field.

DOI: 10.1103/PhysRevLett.109.197001 PACS numbers: 74.20.Rp, 73.20.At, 74.20.Mn, 74.70.Wz

Graphene, a single layer of carbon, has generated immense interest ever since its experimental discovery [1]. Lately, experimental advances in doping methods [2,3] have allowed the electron density to approach the van Hove singularities (VHSs) at 25% hole or electron doping. The logarithmically diverging density of states at the VHS can allow nontrivial ordered ground states to emerge due to strongly enhanced effects of interactions. Very recently, both perturbative renormalization group [4] and functional renormalization group calculations [5,6] have shown that a chiral spin singlet $d_{x^2-y^2} + id_{xy}$ ($d_1 + id_2$) superconducting state likely emerges from electron-electron interactions in graphene doped to the vicinity of the VHS. This is in agreement with earlier studies of strong interactions on the honeycomb lattice near half filling [7–10].

Rather unique to the honeycomb lattice is the degeneracy of the two d-wave pairing channels [7,11]. Below the superconducting transition temperature (T_c), this degeneracy results in the time-reversal symmetry breaking $d_1 + id_2$ state [4,7]. However, any imperfections, and most notably edges, might destroy this degeneracy and generate a local superconducting state different from that in the bulk. At the same time, many of the exotic features proposed for a $d_1 + id_2$ superconductor, such as spontaneous [12,13], or even quantized [14], edge currents and quantized spin- and thermal Hall effects [15,16], are intimately linked to its edge states. In order to determine the properties of $d_1 + id_2$ superconducting graphene, it is therefore imperative to understand the effect of edges on the superconducting state.

In this Letter, we establish the edge properties of $d_1 + id_2$ superconducting graphene doped to the vicinity of the VHS. We show that, while the bulk is in a $d_1 + id_2$ state, any edge will be in a pure, and enhanced, d_1-wave state. Because of a very long decay length of the edge d_1 state, the edges influence even the properties of macroscopic graphene samples. We find two well-localized chiral edge modes which carry a spontaneous, but not quantized, edge current. Furthermore, we show that, by including a realistic Rashba spin-orbit coupling, graphene can be tuned, by using a Zeeman field, to host a Majorana fermion at the edge. These results establish the exotic properties of the chiral $d_1 + id_2$ superconducting state in doped graphene, which, if experimentally realized, will provide an exemplary playground for topological superconductivity. Furthermore, these results are also very important for any experimental scheme aimed at detecting the $d_1 + id_2$ state in graphene, as such a scheme will likely be based on the distinctive properties of the edge.

We approximate the π-band structure of graphene as

$$H_0 = -t \sum_{\langle i,j\rangle,\sigma} c^\dagger_{i\sigma} c_{j\sigma} + \mu \sum_{i} c^\dagger_{i\sigma} c_{i\sigma}, \tag{1}$$

where $t = 2.5$ eV is the nearest-neighbor (NN) hopping amplitude and $c_{i\sigma}$ is the annihilation operator on site i with spin σ. The chemical potential is μ, and the VHS appears at $\mu = \pm t$, where the Fermi surface transitions from being centered around K, K' to Γ. We study two different models for superconducting pairing from repulsive electron-electron interactions:

$$H_\Delta = \sum_{i,\alpha} \Delta_\alpha(i)(c^\dagger_{i\uparrow} c^\dagger_{i+a_\alpha\downarrow} - c^\dagger_{i\downarrow} c^\dagger_{i+a_\alpha\uparrow}) + \text{H.c.} \tag{2}$$

In the limit of very strong on-site Coulomb repulsion, (mean-field) pairing appears on NN bonds such that $a_\alpha = \delta_\alpha$ ($\alpha = 1, 2, 3$) [7], whereas a moderate on-site repulsion gives rise to pairing on next-nearest-neighbor (NNN) bonds with $a_\alpha = \gamma_\alpha$ [5]; see Fig. 1(a). The high electron density near the VHS efficiently screens long-range electron-electron interactions, and we also show that our results are largely independent of the choice of a. In mean-field theory the order parameter can be calculated from the condition $\Delta_\alpha(i) = -J\langle c_{i\downarrow} c_{i+a_\alpha\uparrow} - c_{i\uparrow} c_{i+a_\alpha\downarrow}\rangle$. Here J is the effective (constant) pairing potential arising from the electron-electron interactions and residing on NN bonds for $a = \delta$ and on NNN bonds for $a = \gamma$. By using this

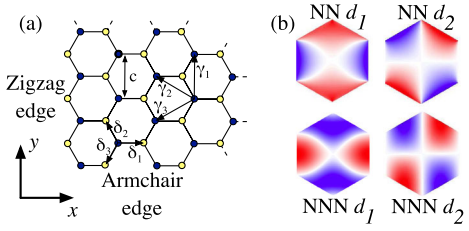

FIG. 1 (color online). (a) Graphene with NN bonds δ_α, NNN bonds γ_α, and zigzag and armchair edges indicated. (b) Different d-wave superconducting order parameters for NN and NNN pairing with negative (blue) and positive (red) sign.

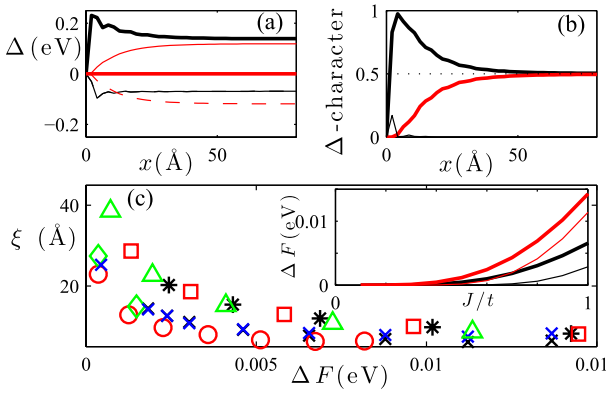

FIG. 2 (color online). (a) Order parameter profile for the zigzag edge for NN $J = 0.75t$ at the VHS with real (black lines) and imaginary (red lines) parts for Δ_1 (thick line), Δ_2 (thin line), and Δ_3 (dashed line) [the black dashed line is hidden behind the black solid line since $\mathrm{Re}(\Delta_2) \approx \mathrm{Re}(\Delta_3)$]. (b) Character of the order parameter in (a): d_1 (thick black line), d_2 (thick red line), and s (thin black line). The dotted line marks the bulk value. (c) Decay length ξ of the d_1 character as a function of ΔF for different doping levels, edges, and superconducting pairing: NN pairing, zigzag edge, and $\mu = t$ (black cross), $\mu = 0.8t$ (red circle), $\mu = 1.2t$ (green diamond), or armchair edge and $\mu = t$ (blue cross), NNN pairing, zigzag edge, and $\mu = t$ (black asterisk), $\mu = 0.8t$ (red square), $\mu = 1.2t$ (green upward triangle) [blue, cross symbols are often completely overlaying black, cross symbols since no notable difference is found between zigzag and armchair edges]. The inset shows ΔF as a function of the pairing potential for NN pairing (black lines) and NNN pairing (red lines) for $\mu = t$ (thick line) and $\mu = 1.2t$ (thin line). $\mu < t$ has a ΔF curve similar to $\mu > t$.

condition for Δ, the Hamiltonian $H = H_0 + H_\Delta$ can be solved self-consistently within the Bogoliubov–de Gennes formalism [17,18]. The favored bulk solution of Δ_α belongs to the two-dimensional E_2 irreducible representation of the $\mathcal{C}_{6v}$ lattice point group. This representation can be expressed in the basis $\hat{\mathbf{a}}_{d_1} = (1, -\frac{1}{2}, -\frac{1}{2})$, which has $d_1 = d_{x^2-y^2}$ symmetry when H_0 is diagonal, and $\hat{\mathbf{a}}_{d_2} = (0, \frac{\sqrt{3}}{2}, -\frac{\sqrt{3}}{2})$, which has $d_2 = d_{xy}$ symmetry; see Fig. 1(b). In the translational invariant bulk, these two solutions have the same T_c, but below T_c the complex combination $d_1 + id_2$ has the lowest free energy [4,7]. There is also an s-wave solution, $\hat{\mathbf{a}}_s = (1, 1, 1)$, but it appears only subdominantly and at very strong pairing.

In order to quantify the edge effects, we study thick ribbons with both zigzag and armchair edges. We assume smooth edges and Fourier transform in the direction parallel to the edge. Because of computational limitations, we need $J \gtrsim 0.5t$ in order to reach bulk conditions inside the slab. This gives rather large Δ_α, but by studying the J dependence we can nonetheless draw conclusions for the experimentally relevant low-J regime.

Superconducting state at the edge.—In the bulk, the $d_1 + id_2$ state has a free energy ΔF lower than the $d_{1,2}$ states, which varies strongly with both doping and pairing potential; see the inset in Fig. 2(c). However, sample edges break the translational invariance, and a qualitatively different solution emerges. Figure 2(a) shows how the zigzag edge completely suppresses the imaginary part of Δ_α while at the same time enhancing the magnitude. This suppression leads to a pure d_1 solution at the edge, an effect we quantify in Fig. 2(b) by plotting the d_1 character $|\frac{\sqrt{2}}{\sqrt{3}}[\Delta_1 - \frac{1}{2}(\Delta_2 + \Delta_3)]|^2$. The edge behavior can be understood by noting that bonds δ_2 and δ_3 (γ_2 and γ_3) are equivalent for both armchair and zigzag edges [19], and, therefore, the d_1-wave state is heavily favored at both types of edges. Since the edge is of the zigzag type for edges with 30° and 90° angles off the x axis and of the armchair type for 0° and 60° angles, we conclude that any edge should host d-wave order with nodes angled 45° from the edge direction. In order to quantify the spatial extent of this edge effect, we calculate a decay length ξ by fitting the d_1-character profile to the functional form $(Ce^{-x/\xi} + 0.5)$ with $C \approx 0.5$. As seen in Fig. 2(c), ξ varies strongly with ΔF but very little with edge type and doping level. Furthermore, the increase in ξ for NNN pairing compared to NN pairing suggests that the edge will be even more important in models with longer ranged Coulomb repulsion. The strongly increasing ξ with decreasing ΔF has far-reaching consequences for graphene. For example, $J = 0.5t$ and doping at the VHS gives $\xi \approx 25$ Å for NN pairing. With an expected much weaker superconducting pairing in real graphene, the edge will modify the properties of the superconducting state not only in graphene nanoribbons but also in macroscopically sized graphene samples. We have verified that both the $d_1 + id_2$ state itself and edge effects described here are stable in the presence of random disorder (see Supplemental Material [18]).

Chiral edge states.—Any $d_1 + id_2$ state, even with one subdominant part, violates both time-reversal and parity symmetry and has been shown to host two chiral edge states [12,14,15]. The topological invariant guaranteeing the existence of these two chiral edge modes also causes quantized spin- and thermal-Hall responses [15,16]. Figure 3(a) shows the band structure for a zigzag slab. The self-consistent solution (thick black line) gives two Dirac cones located at $\pm k_0$, where bands with same

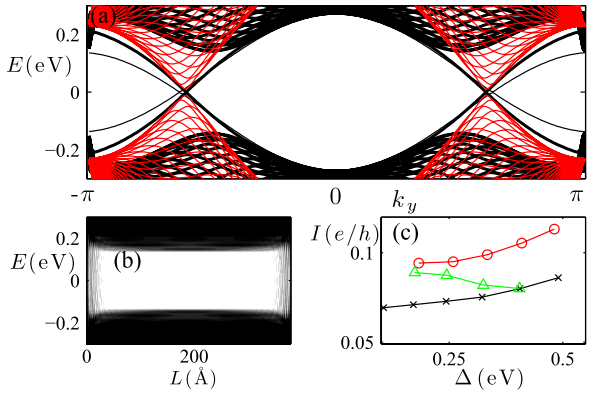

FIG. 3 (color online). (a) Band structure for a zigzag edge slab with NN $J = 0.75t$, $\mu = t$, and self-consistent Δ (thick black line), constant $d_1 + id_2$ state corresponding to the bulk state (thin black line), and constant d_1 state corresponding in amplitude to the d_1 state at the surface. (b) LDOS across the ribbon for the self-consistent solution in (a) interpolating between 0.2 (black) to 0 (white) states/(eV unit cell), showing a bulk gap of 0.18 eV and gapless edge states. (c) Quasiparticle edge current in units of e/h as a function of superconducting bulk order parameter $\Delta(1, e^{2\pi i/3}, e^{4\pi i/3})$ for the zigzag edge with $\mu = t$ (black cross) and $\mu = 0.8t$ (red circle) and the armchair edge with $\mu = t$ (green upward triangle).

velocities reside on the same surface, thus yielding two copropagating chiral surface states per edge. The band structure for the constant (nonself-consistent) bulk $d_1 + id_2$ state also has two Dirac cones (thin black line) but shifted away from k_0. The shift is directly related to the d_1 state at the edge. The d_1 state has no surface states on the zigzag edge, only bulk nodal quasiparticles, where the nodes for a d_1 order parameter with amplitude equal to that on the edge are located at $\pm k_0$ (thin red line). The similarity between the $d_1 + id_2$ and d_1 edge band structures thus makes for only modest effects of the edge on the self-consistent band structure. It also results in the chiral edge modes being well-localized to the edge, as seen in the local density of states (LDOS) plot in Fig. 3(b). The constant edge LDOS is a consequence of the one-dimensional Dirac spectrum. We note especially that no d-wave superconducting graphene edge will display a zero-bias conductance peak due to zero-energy surface states, in contrast to the cuprate superconductors [13]. Such a peak is present only when the order parameter for incidence angle θ on the edge has a different sign from when the angle is $\pi - \theta$. This happens only for the d_2 solution on both the zigzag and armchair edge.

The breaking of time-reversal symmetry gives rise to spontaneous edge currents carried by the chiral edge modes [12–14,16]. By combining the charge continuity equation with the Heisenberg equation for the particle density [17], we calculate in Fig. 3(c) the quasiparticle edge current as a function of the bulk order parameter $\Delta(1, e^{2\pi i/3}, e^{4\pi i/3})$. We find no evidence for a quantized boundary current equal to $2e\Delta/h$, as previously suggested [14]. In fact, we find a nonlinear relationship between the current and Δ, a strong variation with doping level, and, most importantly, the armchair current even decreases when Δ increases. The last result can be understood by studying the zero-energy crossing $\pm k_0$ of the chiral edge modes. For the zigzag edge k_0 increases with increasing Δ, whereas for the armchair edge k_0 decreases. In general, we find that changes in current are proportional to δk_0^β with $\beta \approx 1 - 2$. This, at least, partially agrees with earlier results reporting a $\beta = 2$ dependence [12]. Finite k-point sampling and neglecting the screening supercurrents could potentially explain the discrepancy.

Majorana mode.—Heavy doping of graphene, by either adatom deposition [2] or gating [3], breaks the $z \to -z$ mirror symmetry and introduces a Rashba spin-orbit coupling [20]:

$$H_\lambda = i\lambda_R \sum_{\langle i,j\rangle,\sigma,\sigma'} \hat{\mathbf{z}} \cdot (\mathbf{s}_{\sigma,\sigma'} \times \hat{\mathbf{d}}_{ij}) c_{i\sigma}^\dagger c_{j\sigma'}, \tag{3}$$

where $\hat{\mathbf{d}}_{ij}$ is the unit vector from site j to i. Superconducting two-dimensional systems with Rashba spin-orbit coupling and magnetic field have recently attracted much attention due to the possibility of creating Majorana fermions at vortex cores or edges [21–23]. At edges the Majorana fermion appears as a single mode crossing the bulk gap. This should be contrasted with the behavior found above, where the edge instead hosts two modes. We will here show that a Majorana mode is created in d-wave superconducting doped graphene in the presence a moderate Zeeman field: $H_h = -h_z \sum_i (c_{i\uparrow}^\dagger c_{i\uparrow} - c_{i\downarrow}^\dagger c_{i\downarrow})$. Because of spin mixing in H_λ, the basis vector $X^\dagger = (c_{i\uparrow}^\dagger c_{i\downarrow}^\dagger c_{i\uparrow} c_{i\downarrow})$ has to be used when expressing the Hamiltonian $H_{\text{ext}} = H_0 + H_\Delta + H_\lambda + H_h$ in matrix form: $H_{\text{ext}} = \frac{1}{2} X^\dagger \mathcal{H}_{\text{ext}} X$. This results in a doubling of the number of eigenstates compared to the physical band structure. This doubling is necessary for the appearance of the Majorana fermion, since a regular fermion consists of two Majorana fermions.

A change in the number of edge modes marks a topological phase transition which, in general, can occur only when the bulk energy gap closes. We therefore start by identify the conditions for bulk zero energy solutions of H_{ext}. Close to the VHS we can, to a first approximation, use only the partially occupied π band for small Δ, λ_R, and h_z. A straightforward calculation [23] for this one-band Hamiltonian gives the following bulk-gap closing conditions at $\mu \sim t$:

$$\begin{aligned} (\mu - t|\epsilon_k|)^2 + \Delta_k^2 &= h_z^2 + \lambda_R^2 |\mathcal{L}_k|^2, \\ |\Delta_k||\lambda_R \mathcal{L}_k| &= 0, \end{aligned} \tag{4}$$

where $\epsilon_k = \sum_\alpha e^{ik\delta_\alpha}$ is the band structure, $\varphi_k = \arg(\epsilon_k)$, $\Delta_k = -\sum_\alpha \Delta_\alpha \cos(k\delta_\alpha - \varphi_k)$ is the k-dependent intraband superconducting order for NN pairing [7],

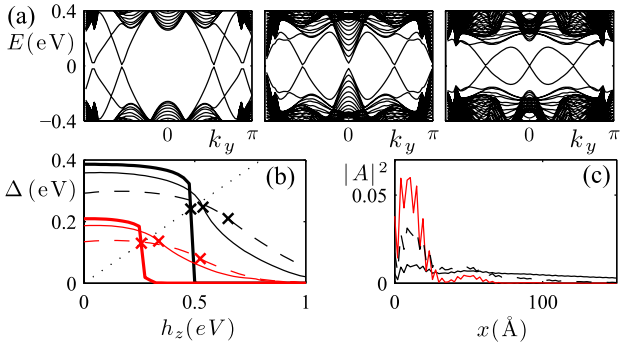

FIG. 4 (color online). (a) Eigenvalue spectrum for a zigzag slab with NN $J = 1.2t$, $\mu = t$, $\lambda_R = 0.2t$, and $h_z = 0.4$, 0.535, and 0.6 eV (left to right), with $h_c = 0.535$ eV. Small gaps in the surface states are due to limited k-point sampling. (b) Self-consistent Δ as a function of h_z for $J = 1.2t$ (black line) and $0.9t$ (red line) for $\lambda_R = 0.05t$ (thick line), $0.2t$ (thin line), and $0.3t$ (dashed line). The dotted line marks the $h_c = 2\Delta$ one-band model phase transition. Crosses mark the numerical phase transition. (c) Eigenvalue amplitude squared for the Majorana mode in (a) for $h_z = 0.54$ eV (black line), 0.56 (dashed line), and 0.6 (red line).

and $\mathcal{L}_k = \mathrm{Im}[e^{-i\varphi_k}(-\frac{\sqrt{3}}{2}e^{ik\delta_2} + \frac{\sqrt{3}}{2}e^{ik\delta_3}, e^{ik\delta_1} - \frac{1}{2}e^{ik\delta_2} - \frac{1}{2}e^{ik\delta_3}, 0)]$ is the spin-orbit interaction when expressed in the form $H_\lambda = \sum_{k\sigma\sigma'}\lambda_R\mathcal{L}_k \cdot \mathbf{s}_{\sigma\sigma'}c^\dagger_{k\sigma}c_{k\sigma'}$ for the one-band model. Equations (4) are met at Γ, K, and M in the Brillouin zone, where they produce the conditions $(\mu - 3t)^2 = h_z^2$, $\mu^2 = h_z^2$, and $(\mu - t)^2 + \Delta_k^2(M) = h_z^2$, respectively. At $\mu \sim t$ only the last condition is satisfied for small h_z, which is necessary for superconductivity to survive. We find $\Delta_k(M) = 2\Delta$ for the $\Delta(1, e^{2\pi i/3}, e^{4\pi i/3})$ order parameter, and, thus, at the VHS there is a topological phase transition at $h_c = 2\Delta$. Figure 4(a) shows how the eigenvalue spectrum of a superconducting zigzag slab at the VHS develops when h_z is swept past h_c. At finite λ_R and/or h_z the chiral modes in Fig. 3(a) split with one mode moving towards $k_y = 0$ and the other one towards the zone boundary at $k_y = \pi$; see the leftmost figure in Fig. 4(a). At h_c (center figure) the bulk gap closes at both $k_y = 0$, π. The closure at $k_y = \pi$ annihilates the outer chiral modes, whereas the closure at $k_y = 0$ leaves a new Dirac cone crossing the bulk band gap with the two modes belonging to different edges. Thus, at $h_z > h_c$ we are left with three modes per edge crossing the bulk gap. The odd number establishes the existence of a Majorana mode alongside the two remnant chiral modes. Figure 4(b) shows how Δ develops in the presence of an applied Zeeman field h_z, with $\times$-symbols marking the phase transition into the phase with a Majorana fermion. The dotted line marks the one-band result $h_c = 2\Delta$, which is a good approximation for small λ_R. In this small λ_R regime, there is a very pronounced drop in Δ at the phase transition with only a small remnant superconducting state in the Majorana phase at $h_z > h_c$, which results in a poorly resolved Majorana mode. Larger λ_R gives a stronger superconducting state in the Majorana phase. However, for $\lambda_R > 0.2t$ we find $h_c > 2\Delta$, and the superconducting state is again very weak beyond the phase transition. We thus conclude that, in order to create a Majorana fermion at the edge of d-wave superconducting graphene doped very close to the VHS, a small to moderate Rashba spin-orbit coupling, $\lambda_R \sim 0.2t$, and a Zeeman field of the order of 2Δ are needed. With reported tunability with electric field [24], as well as impurity-induced Rashba spin-orbit coupling [25], $\lambda_R \sim 0.2t$ is likely within experimental reach in heavily doped graphene. The Zeeman field can be generated by proximity to a ferromagnetic insulator, whereas, if applying an external magnetic field, orbital effects also need to be taken into account. Finally, in Fig. 4(c), we plot the spatial profile of the Majorana mode amplitude just beyond h_c. Because of the larger Δ at the edge, the bulk enters the Majorana-supporting topological phase before the edge. Therefore, the Majorana mode does not appear at the edge but is spread throughout the sample for $h_z \gtrsim h_c$. Not until $h_z > 2\Delta$(edge) does the Majorana mode appear as a pure edge excitation.

In summary, we have shown that the $d_1 + id_2$ superconducting state in heavily doped graphene is in a pure d_1 state on any edge. The d_1 edge state significantly modifies the superconducting state even in macroscopic graphene samples due to a long decay length. Moreover, $d_1 + id_2$ superconducting graphene hosts two well-localized chiral edge modes, which carry a nonquantized spontaneous quasiparticle current. A Majorana mode can also be created at the edge by tuning a moderate Zeeman field. These results establish the properties of the $d_1 + id_2$ state in graphene and will be important for any experimental detection of this state.

The author thanks A. V. Balatsky, M. Fogelström, and T. H. Hansson for discussions and the Swedish research council (VR) for support.

[1] K. S. Novoselov, A. K. Geim, S. V. Morozov, D. Jiang, Y. Zhang, S. V. Dubonos, I. V. Grigorieva, and A. A. Firsov, Science **306**, 666 (2004).
[2] J. L. McChesney, A. Bostwick, T. Ohta, T. Seyller, K. Horn, J. González, and E. Rotenberg, Phys. Rev. Lett. **104**, 136803 (2010).
[3] D. K. Efetov and P. Kim, Phys. Rev. Lett. **105**, 256805 (2010).
[4] R. Nandkishore, L. S. Levitov, and A. V. Chubukov, Nat. Phys. **8**, 158 (2012).
[5] M. L. Kiesel, C. Platt, W. Hanke, D. A. Abanin, and R. Thomale, Phys. Rev. B **86**, 020507(R) (2012).
[6] W.-S. Wang, Y.-Y. Xiang, Q.-H. Wang, F. Wang, F. Yang, and D.-H. Lee, Phys. Rev. B **85**, 035414 (2012).
[7] A. M. Black-Schaffer and S. Doniach, Phys. Rev. B **75**, 134512 (2007).

[8] C. Honerkamp, Phys. Rev. Lett. **100**, 146404 (2008).
[9] S. Pathak, V. B. Shenoy, and G. Baskaran, Phys. Rev. B **81**, 085431 (2010).
[10] T. Ma, Z. Huang, F. Hu, and H.-Q. Lin, Phys. Rev. B **84**, 121410(R) (2011).
[11] J. González, Phys. Rev. B **78**, 205431 (2008).
[12] G. E. Volovik, JETP Lett. **66**, 522 (1997).
[13] M. Fogelström, D. Rainer, and J. A. Sauls, Phys. Rev. Lett. **79**, 281 (1997).
[14] R. B. Laughlin, Phys. Rev. Lett. **80**, 5188 (1998).
[15] T. Senthil, J. B. Marston, and M. P. A. Fisher, Phys. Rev. B **60**, 4245 (1999).
[16] B. Horovitz and A. Golub, Phys. Rev. B **68**, 214503 (2003).
[17] A. M. Black-Schaffer and S. Doniach, Phys. Rev. B **78**, 024504 (2008).
[18] See Supplemental Material at http://link.aps.org/supplemental/10.1103/PhysRevLett.109.197001 for more information on disorder effects.
[19] A. M. Black-Schaffer and S. Doniach, Phys. Rev. B **79**, 064502 (2009).
[20] C. L. Kane and E. J. Mele, Phys. Rev. Lett. **95**, 146802 (2005).
[21] J. D. Sau, R. M. Lutchyn, S. Tewari, and S. D. Sarma, Phys. Rev. Lett. **104**, 040502 (2010).
[22] J. Alicea, Phys. Rev. B **81**, 125318 (2010).
[23] M. Sato, Y. Takahashi, and S. Fujimoto, Phys. Rev. B **82**, 134521 (2010).
[24] H. Min, J. E. Hill, N. A. Sinitsyn, B. R. Sahu, L. Kleinman, and A. H. MacDonald, Phys. Rev. B **74**, 165310 (2006).
[25] A. H. C. Neto and F. Guinea, Phys. Rev. Lett. **103**, 026804 (2009).